analytical chemistry

Article

pubs.acs.org/ac

Imaging Mass Spectrometry of Diversified Cardiolipin Molecular Species in the Brain

A. A. Amoscato,*[,†,‡,#] L. J. Sparvero,[†,‡,#] R. R. He,[†,‡,⊥] S. Watkins,[∥] H. Bayir,*[,†,‡,§] and V. E. Kagan*[,†,‡]

[†]Department of Environmental and Occupational Health, [‡]Center for Free Radical and Antioxidant Health, [§]Department of Critical Care Medicine and Safar Center for Resuscitation Research, and [∥]Department of Cell Biology, University of Pittsburgh, Pittsburgh, Pennsylvania 15219, United States

[⊥]Pharmacy College, Jinan University, Guangzhou, Guangdong 510632, China

Supporting Information

ABSTRACT: MALDI imaging mass spectrometry (MALDI-IMS) has been used successfully in mapping different lipids in tissue sections, yet existing protocols fail to detect the diverse species of mitochondria-unique cardiolipins (CLs) in the brain which are essential for cellular and mitochondrial physiology. We have developed methods enabling the imaging of individual CLs in brain tissue. This was achieved by eliminating ion suppressive effects by (i) cross-linking carboxyl/amino containing molecules on tissue with 1-ethyl-3-[3-(dimethylamino)propyl]-carbodiimide hydrochloride and (ii) removing highly abundant phosphatidylcholine head groups via phospholipase C treatment. These treatments allowed the detection of CL species at 100 μm resolution and did not affect the amount or molecular species distribution of brain tissue CLs. When combined with augmented matrix application, these modifications allowed the visualization and mapping of multiple CL species in various regions of the brain including the thalamus, hippocampus, and cortex. Areas such as the dentate and stratum radiatum exhibited higher CL signals than other areas within the hippocampal formation. The habenular nuclear (Hb)/dorsal third ventricle (D3 V) and lateral ventricle (LV) areas were identified as CL "hot spots". Our method also allowed structural MS/MS fragmentation and mapping of CLs with identified fatty acid residues and demonstrated a nonrandom distribution of individual oxidizable (polyunsaturated fatty acid containing) and nonoxidizable (nonpolyunsaturated containing) CLs in different anatomical areas of the brain. To our knowledge, this method is the first label-free approach for molecular mapping of diversified CLs in brain tissue.

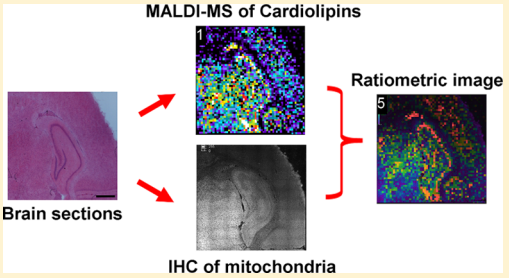

In eukaryotes, the cardiolipins (CL), a class of mitochondrion-specific anionic phospholipids, play multiple structural and functional roles in bioenergetics, mitochondrial signaling, and cellular fate pathways. While the aggregate abundance of CLs in cells and tissues is low relative to other phospholipids (2−3 mol %) within the mitochondrion, about a quarter of the phospholipid molecules in the inner mitochondrial membrane (IMM) is CLs, particularly in the matrix-oriented leaflet. CLs are associated with multiple integral and peripheral mitochondrial proteins, from electron-transporting respirasomes to anion channels and enzymes, and are present in a noncomplexed form, thereby contributing to the extreme curvature of mitochondrial cristae.[1−5] During mitochondrial stress or damage, the asymmetric CL distribution collapses resulting in its externalization to the outer mitochondrial membrane (OMM), leading to signaling events essential for mitophagy and apoptosis.[2,6,7] The general structure of CL (1,3-bis(*sn*-3′-phosphatidyl)-*sn*-glycerol) is a unique dimeric moiety, composed of two phosphatidylglycerols connected via a glycerol backbone, which displays two negative charges from the phosphate groups and four acyl chains. In polyunsaturated CL species, these acyl chains readily undergo enzymatic oxygenation[2] which we have recently identified as a novel generator of lipid mediators in mitochondria.[8]

This extraordinarily significant role in cell and mitochondrial physiology leads to a pressing need to develop quantitative methods to define the isoforms of CL, their dynamics, expression, and of course distribution in tissues. Contemporary liquid-chromatography/mass spectrometry (LC-MS) does allow us to identify, characterize, and quantify individual CLs.[9,10] Unfortunately, no specific or reliable "labels" (fluorescent probes, antibodies) or in fact methods to define and localize the tissue distribution of brain CLs, in total and as subtypes, exists. While variants of imaging mass spectrometry (IMS) have been used to demonstrate the spatial distribution of a number of abundant (phospho)lipids in tissue, there have been no reports on the successful imaging of CLs in brain tissue.[11−13] This is because of the very low abundance of CLs combined with their remarkable diversification and distribution over numerous molecular species in the brain in contrast to many other tissues.[14]

Received: April 2, 2014
Accepted: June 10, 2014
Published: June 10, 2014

   dx.doi.org/10.1021/ac5011876 | *Anal. Chem.* 2014, 86, 6587−6595

Here, we report novel methods for the IMS of different CL species in brain tissue sections which allows label-free spatial resolution. Using this approach, we have (1) visualized and mapped multiple CL species, (2) performed structural MS/MS fragmentation and mapping of CLs with identified fatty acid residues, and (3) demonstrated a nonrandom distribution of individual polyunsaturated fatty acid (PUFA) containing and non-PUFA containing CLs in different anatomical areas of the brain.

EXPERIMENTAL SECTION

Reagents. Chloroform and ethanol (HPLC grade) were purchased from Sigma-Aldrich (St. Louis, MO, USA). Methanol was LC-MS grade from Fisher Scientific (Pittsburgh, PA, USA). Water was purified by a Milli-Q system (EMD Millipore, Billerica, MA, USA). 1-Ethyl-3-[3-(dimethylamino)-propyl]carbodiimide hydrochloride (EDC) was purchased from Thermo Scientific/Pierce Biotechnology (Rockford, IL, USA). Phospholipase C (PLC) from *B. cerus*, ammonium acetate, and 2,5-dihydroxybenzoic acid (DHB) were also purchased from Sigma-Aldrich (St. Louis, MO, USA).

Animals and Tissue Preparation. All procedures were preapproved and performed according to the protocols established by the Institutional Animal Care and Use Committee of the University of Pittsburgh. Brains from 17 day old male Sprague−Dawley rats were harvested and immediately frozen in liquid nitrogen with neither fixation nor embedding and cut immediately. Brain tissue was affixed to a cryotome block with minimal Tissue-Tek OCT (Sakura FineTek USA, Torrance, CA, USA). The blade and working surfaces of the cryotome were cleaned with methanol immediately prior to cutting and at no time did the blade come into contact with OCT. Coronal brain sections from Bregma A 2.3 mm to A 3.2 mm were cut at −21 °C at a thickness of 10 μm. These sections were applied to cold histology slides coated with a conductive indium−tin oxide (ITO) surface (Delta Technologies LTD, Loveland, CO, USA). Additional sections were cut and applied to plain glass slides for immunohistochemistry, hematoxylin and eosin (H&E) staining, and total lipid extraction. Lipid extraction from dried tissue sections on glass slides was performed using the modified Folch method as described previously.[15] Total lipid extracts were dried under a steady stream of grade 5.0 N_2, then redissolved in 2:1 chloroform/methanol to a total volume of 150 μL, and stored at −80 °C prior to use.

In order to apply matrix more homogeneously than airbrushes or TLC sprayers can achieve, we constructed a capillary-sprayer from the electrospray source from a Thermo-Finnigan TSQ 7000 mass spectrometer. The existing capillary was replaced with 75 μm i.d. polyimide coated capillary tubing (Scientific Instrument Services, Ringoes, NJ, USA). Sheath gas (grade 5.0 N_2) was regulated to 80 psi at the output of the nitrogen regulator. Further fine control of nitrogen gas was achieved using a needle valve to maintain a flow rate of 30 L/h. The spray nozzle was placed at 35 mm above the tissue. A syringe pump delivered matrix solution at a rate of 2.0 μL/min. This combination of gas flow, height, and deposition rate gave optimal coverage of the tissue sections. For CL imaging, the tissue was first treated with 50 μL of 500 mM EDC (1-ethyl-3-[3-(dimethylamino)propyl]carbodiimide) in MES buffer (100 mM, pH 3.7) for 2 h at room temperature and washed with 50 mM ammonium acetate buffer (200 μL, pH 6.7). The tissue was then treated with PLC (0.01 units total in 50 μL of 50 mM ammonium acetate buffer, pH 6.7) for 15 min at 37 °C followed by an additional wash with ammonium acetate buffer as described above. After the chemical/enzymatic treatments, the tissue was vacuum-dried for 2 h and DHB matrix (480 mM in chloroform/methanol, 2:1, v/v) was applied in 2 s bursts with 120 s of drying time in between. This comprised one spraying cycle. A total of 20 cycles was applied to the tissue. Spraying in short (2 s) time increments with drying intervals (2 min) in-between each spray aided in controlling solvent effects. A total of 12 brain sections from three different animals was EDC/PLC treated, and matrix was applied to image lipids at 750, 200, 100, and 50 μm resolutions (see below).

Mass Spectrometry Analysis. MALDI-MS and -IMS analyses were performed using Bruker Ultraflex II and UltraFlextreme axial-TOF/TOF mass spectrometers and a Solarix XR FTICR (Fourier transform ion cyclotron resonance) mass spectrometer equipped with a 7.0 T magnet (Bruker Daltonics, Billerica, MA, USA). The Ultraflex was equipped with a 337 nm wavelength N_2 laser operating at a repetition rate of 20 Hz while the UltraFlextreme and Solarix were equipped with 355 nm NdYAG lasers (1000 Hz repetition rate). The MALDI-TOF MS spectra were acquired in reflector mode with a matrix deflection cutoff of 400 Da in both positive and negative polarities over a window of m/z 400−4000. MALDI-FTICR-MS spectra were acquired in negative polarity mode over a window of m/z 300−4000 with 8 megaword transients and a data reduction coefficient of 0.98. MALDI-TOF-MS/MS spectra were acquired in LIFT mode with negative polarity and a mass isolation window of 0.8% of the parent mass. This window size allowed full signal transmission of ions from one CL cluster but gave no signal from adjacent clusters. MALDI-TOF spectra were externally calibrated using a phospholipid mixture while MALDI-FTICR spectra were calibrated using a lock mass on the monoisotopic peak of GM1 (d18:1/18:0, m/z 1544.86944, $[M - H]^-$). MALDI-IMS images from the Ultraflex were acquired at lateral resolutions of either 200, 100, or 50 μm for IMS or 750 μm for MS/MS imaging, with a summation of either 100 (positive mode), 800 (negative mode), or 3000 (MS/MS mode) laser shots per location. MALDI-MS/MS images from the UltraFlextreme were acquired at a lateral resolution of 200 μm with a summation of 2000 laser shots per location. MALDI-FTICR-MS images from the Solarix were acquired at a lateral resolution of 100 μm with an ion accumulation of 300 laser shots per location and one analysis step. Random walking was performed every 10 (Ultraflex), 50 (Solarix), or 200 (Ultraflextreme) laser shots within each location. Spectra from the Ultraflex were acquired with a global attenuator offset of 60% and an attenuator range of 20% of the maximum. Within that range, a laser energy of 40% was used for positive mode and 50% for negative and MS/MS-mode. Spectra from the Ultraflextreme were acquired with a laser focus setting of 1 (minimum) and an attenuator offset of 49% with a range of 51% of the maximum. Within this range, a laser energy of 100% was used. Spectra from the Solarix were acquired with a laser focus setting of 1 (minimum) and an attenuator offset of 0% with a range of 100%. Within this range, a laser energy of 23% was used. MALDI-IMS images were produced from the corresponding spectra which generated a heat map at a given m/z value using FlexImaging 3.0 (Ultraflex) and FlexImaging 4.0 (Ultra-Flextreme and Solarix) software (Bruker Daltonics, Billerica, MA, USA). Heat maps for a given ion were generated with a mass window of ±0.25 Da (TOF) or 0.001 Da (FTICR) and

dx.doi.org/10.1021/ac5011876 | *Anal. Chem.* 2014, 86, 6587−6595

based on relative intensities with root-mean-squared (RMS) normalization (FlexImaging 4.0) or no normalization (FlexImaging 3.0) unless otherwise noted. Spectra from individual imaged areas were analyzed with FlexAnalysis 3.0 (Ultraflex), FlexAnalysis 3.3 (UltraFlextreme), and DataAnalysis 4.1 (Solarix). Spatial overlays of heat maps with histological features were determined by coregistering fiducial markers on optical images acquired from a microscope prior to matrix deposition and consulting *The Rat Brain in Stereotaxic Coordinates*.[16]

LC-MS/MS analyses (to confirm CL structure) were performed on extracts of tissue slices[17] on a Thermo Q-Exactive hybrid quadrupole-orbitrap mass spectrometer (ThermoFisher, Inc., San Jose, CA). CLs were analyzed using a Luna C8 column (2.0 mm (i.d.) × 15 cm, 5 μm, Phenomenex, Inc.) on a Dionex Ultimate 3000 HPLC system (Thermo Fisher Scientific, San Jose, CA). The column compartment was maintained at 30 °C. Solvents consisted of 2-propanol/water/triethylamine/acetic acid (45:5:0.25:0.25, isocratic). For CL quantitation, LC was performed on a Luna Silica column (2.0 mm × 15 cm) using a hexane/propanol/water solvent system (43:57:1, solvent A; 43:57:10, solvent B) containing 10 mM ammonium acetate. Gradient: 10−37% B in 15 min; 37−65% B in 8 min and 65−100% B in 2 min; hold at 100% B for 22 min. Tetramyristoyl CL (TMCL) was used as an internal standard. Flow was maintained at 0.2 mL/min. Analysis was performed in negative ion mode at a resolution of 140,000 for the full MS scan and 35,000 for the MS^2 scan in a data-dependent mode. The scan range for MS analysis was 1200−1600 m/z with a maximum injection time of 100 ms using 1 microscan. A maximum injection time of 128 ms was used for MS^2 (high energy collisional dissociation (HCD)) analysis with collision energy set to 24. An isolation window of 1.0 and 0.5 Da was set for the MS and MS^2 scans, respectively. Capillary spray voltage was set at 4.0 kV, and capillary temperature was 320 °C.

Immunohistochemistry and Fluorescent Imaging of Mitochondria in Rat Brain Tissue Sections. Thin (10 μm) frozen sections were cut, mounted on slides, labeled with antibodies to TOM 20 (cat. # sc-11415/A3113, Santa Cruz Biotechnology, Inc., Dallas, TX), nuclei counter stained with Hoescht dye, and mounted as previously described.[18] Entire sections were scanned, and images were collected using a Nikon 90i (Melvillen, NY, USA) upright microscope, 20× dry plan apochromat objective, and motorized stage. Individual images were stitched together using Nikon Elements software. To overlay the MALDI-IMS data with the immunocytochemical data, fiduciary structures common to the semiserial IMS and light microscopy images were identified. The MALDI-IMS images were resized such that the pixel count matched that of the light microscopy images and images combined into a single file. Various additive combinations of the MALDI-IMS images were made and rendered to the same bit depth (12 bit) as the light microscopy images and ratios calculated of MALDI-IMS intensity/mitochondrial label intensity generated. These images are displayed as pseudocolored images with a ratio between 0 and 2.

RESULTS AND DISCUSSION

Treatment with EDC and PLC Enables the Detection of CL in Rat Brain Tissue. MALDI-IMS has been used to define the localization of multiple classes of lipids in frozen tissue sections, with the brain being the preferred tissue.[19−29] Established conventional methods using 2,5-DHB as the matrix provide precise lipid mapping and spectra (Supplementary Figure 1a, Supporting Information) for multiple classes in the negative ion mode including phosphatidylserines (PS), phosphatidylinositols (PI), sulfatides (ST), and gangliosides in the m/z range of 700−2,000. However, the m/z range of 1,400−1,600, in which CLs exist is predominately populated by signals from ganglioside GM1 (Supplementary Figure 1a, Supporting Information) and is devoid of signals from any CL species (Figure 1a).

We reasoned that the inability to detect CLs was due in part to the ion suppression of the limited CL signals by other more abundant lipid ions such as phosphatidylcholine (PC) and further by the highly abundant and easily ionized carboxyl and amino groups of proteins and other lipids. Accordingly, we

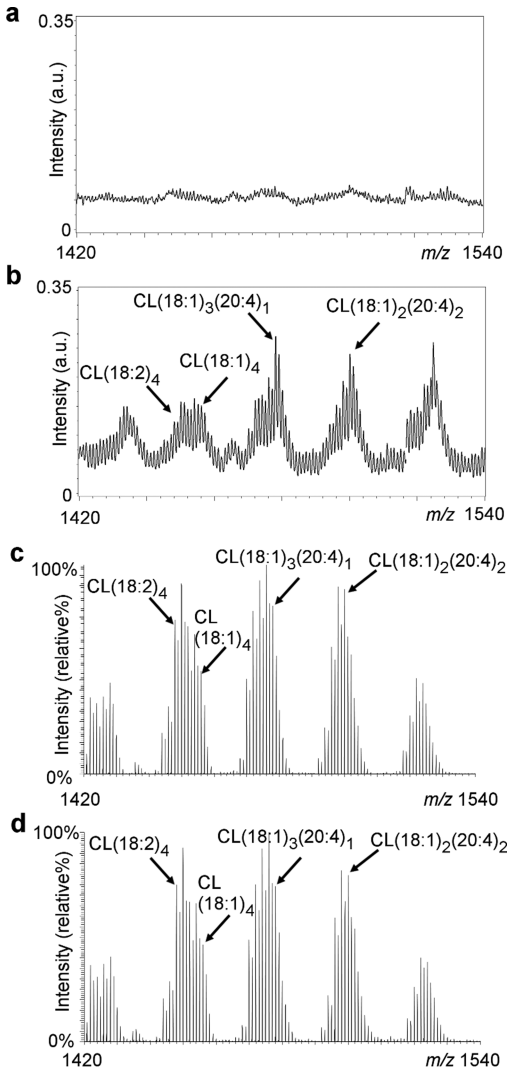

Figure 1. MALDI-IMS and LC-MS spectra of untreated (a,c) and EDC/PLC-treated (b,d) rat brain tissue. MALDI spectra in the CL region, m/z 1420−1540, directly from untreated (a) and EDC-PLC treated (b) tissue sections display a strong increase in signal for CL as a result of EDC-PLC treatment. LC-MS of total lipid extracts from untreated (c) and treated (d) tissue verify that the treatment does not significantly affect the composition of tissue CL. A range of m/z 1420−1540 was chosen because the IMS spectrum (see Supplemental Figure 1a, Supporting Information) was dominated by ganglioside signals beyond m/z 1540. However, additional CL clusters were noted in the region beyond m/z 1540 for the LC-MS spectrum.

dx.doi.org/10.1021/ac5011876 | *Anal. Chem.* 2014, 86, 6587−6595

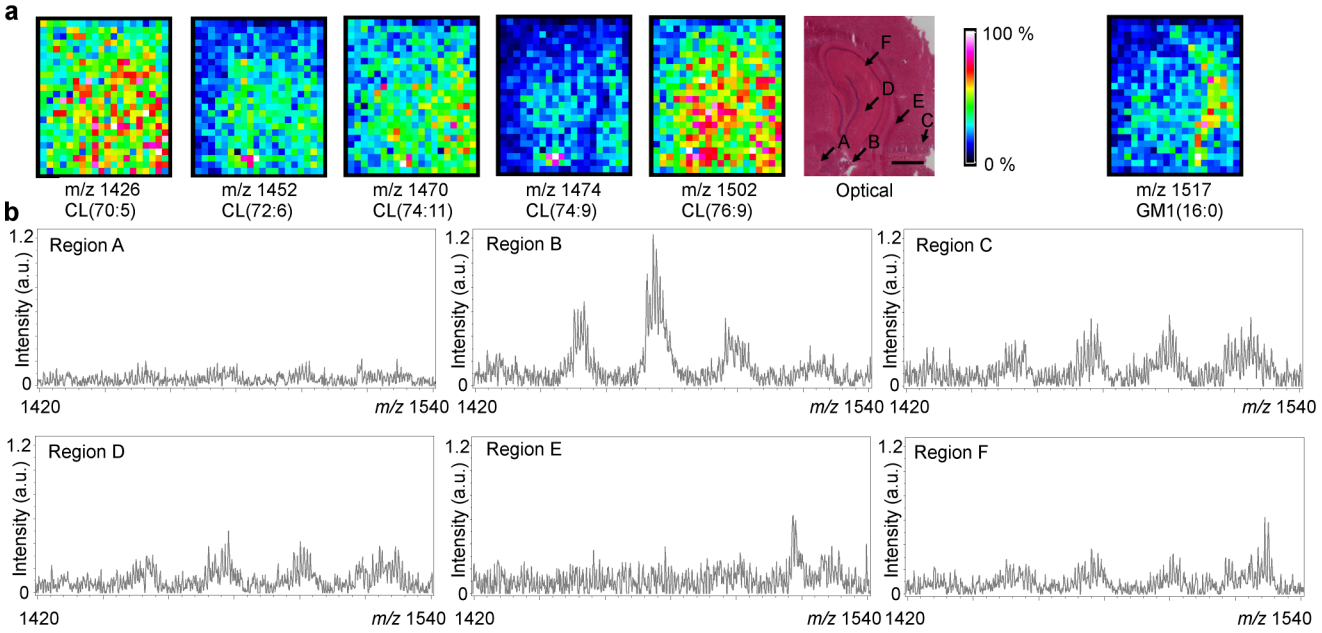

Figure 2. Mapping the spatial distribution of CL species in rat brain. (a) Relative-intensity heat maps of select CL species (m/z 1426, 1452, 1470, 1474, and 1502) from EDC-PLC treated rat brain coronal sections (right hemisphere). An optical image and a heat map of ganglioside GM1 (m/z 1517) are included for comparison. Parentheses indicate CL fatty acyl chain carbon number and the number of double bonds, respectively. Scale bar = 1 mm. Spatial resolution = 200 μm. (b) CL spectra were obtained from one individual pixel from each of the representative anatomical regions (arrows, optical image) from rat brain. These include the medial dorsal thalamic nuclear (region A), the habenular nuclear (Hb) and dorsal 3rd ventricle (D3 V) (region B), the retrosplenial cortex (region C), the dentate gyrus (DG) (region D), the external capsule white matter (region E), and the CA2 regions (region F).

introduced two major modifications to conventional protocols: (i) chemical cross-linking of the tissue surface with 1-ethyl-3-[3-(dimethylamino)propyl]carbodiimide hydrochloride (EDC) and (ii) treatment with phospholipase C (PLC). EDC cross-links accessible carboxyl and amino groups on tissue and hence limits ionization. PLC limits highly abundant/ionizable PC signals by removal of cationic head groups. Although no gross morphological changes were noted, it is possible that, when the EDC and PLC treatments are utilized in tandem, they may induce a complex reorganization of the tissue surface which aids in CL detection by MALDI-IMS. Other major changes included a modification of the matrix application methods by construction of a spraying device that allowed for improved control of the matrix deposition on tissue. We chose the matrix 2,5-DHB in combination with a chloroform/methanol solvent system. This protocol allowed visualization and mapping of multiple CLs in brain tissue (Figure 1b) centering around CL clusters of m/z 1426 $[(16:1)_1/(18:2)_1/(18:1)_2]$, 1450 $[(18:1)_1/(18:2)_3]$, 1476 $[(18:1)_2/(18:2)_1/(20:4)_1]$, 1500 $[(18:1)_2/(20:4)_2$; $(18:0)_1/(18:2)_2/(22:6)_1]$, and 1524 $[(18:1)_2/(20:4)_1/(22:6)_1]$, the same major CL clusters detectable by LC-MS (Figure 1c). Near unit mass resolution was achieved in the MALDI imaging spectra allowing the mapping of various brain CLs. With a spatial resolution of 200 μm (Bruker Ultraflex II), a good compromise between heat map and spectral quality was achieved. While imaging at higher spatial resolutions (100 and 50 μm) was possible, it also resulted in a significant decrease in CL signals (Supplementary Figure 2, Supporting Information).

This approach afforded heat maps and spectra of brain CLs. A comparison of CL spectra from treated and untreated tissue indicated that there were no significant differences in CL molecular species (Figure 1c,d) after EDC/PLC treatment. The treated tissue displayed the same five clusters of CL as the untreated tissue. When quantitative analysis was performed, the amount of endogenous CL remained essentially unchanged (3.3 ± 0.24 pmol/nmol Pi, untreated vs 3.1 ± 0.17 pmol/nmol Pi, EDC/PLC treated) as determined by LC/MS in the presence of TMCL (internal standard). Signals of other lipids in the negative ion mode included sulfatides (STs), phosphatidylinositols (PIs), and gangliosides GM1 and GD1 (Supplementary Figure 1a and Supplementary Table 1b, Supporting Information). One exception was the isobaric species at m/z 834.6 (phosphatidylserine (PS) and ST, Supplementary Figure 1a, Supporting Information). Here, the decreased signal was due to an inability of PS to ionize as a result of the EDC coupling reaction. In positive mode imaging, EDC/PLC-treated tissue displayed the same positive mass ions as the untreated tissue albeit at a much lower signal intensity (Supplementary Figure 3a,b,c and Supplementary Table 1a, Supporting Information). Essentially, PC signals were decreased most significantly followed by PE, the latter due to EDC cross-linking. However, each modification of the EDC/PLC protocol was essential as omission of any treatment was associated with a decrease or loss of CL signal.

Mapping the Spatial Distribution of CL Molecular Species in Rat Brain Tissue. This innovative protocol allowed the previously impossible comparison of the distribution of 21 CL species within several CL clusters in brain subregions (Figure 2a and Supplementary Figure 1b, Supporting Information). Overall, higher intensities of CLs mapped to centrally located areas, such as the dentate and stratum radiatum, within the hippocampal formation. Higher mass CL species (m/z 1476, 1496, 1500, and 1502) also produced signals in the cortical region and while CLs were present in the white matter their signals were much reduced.

dx.doi.org/10.1021/ac5011876 | Anal. Chem. 2014, 86, 6587−6595

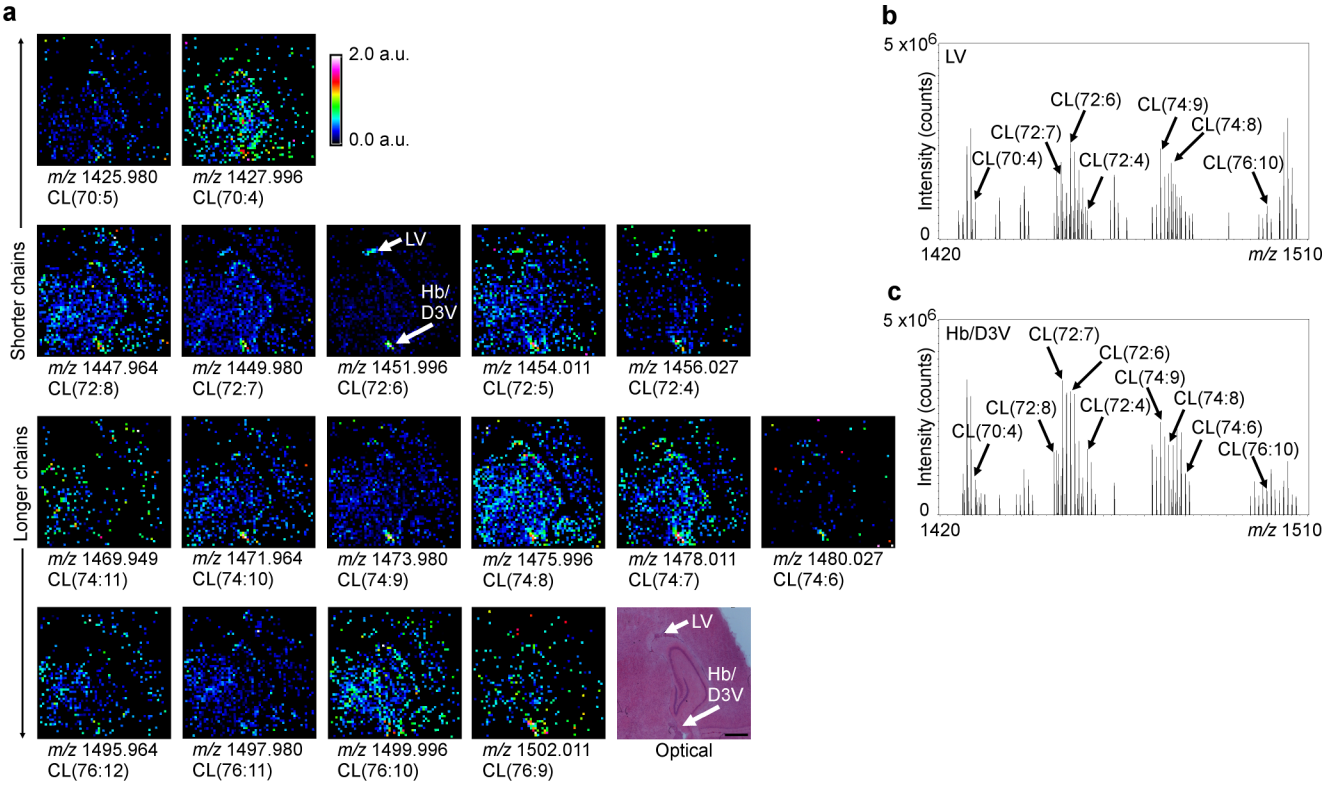

Figure 3. FTICR MALDI IMS of CL species from rat brain. (a) Heat maps of 17 individual CL species from an EDC-PLC treated rat brain coronal section (right hemisphere). An optical image is included for comparison. Parentheses indicate CL fatty acyl chain carbon number and the number of double bonds, respectively. Scale bar = 1 mm. Spatial resolution = 100 μm. (b) Generated spectrum from the lateral ventricle (LV) area. (c) Generated spectrum from the Hb/D3 V area. The associated high resolution mass spectra were generated from a single 100 μm pixel from the LV and Hb/D3 V regions (arrows, optical and heat map image).

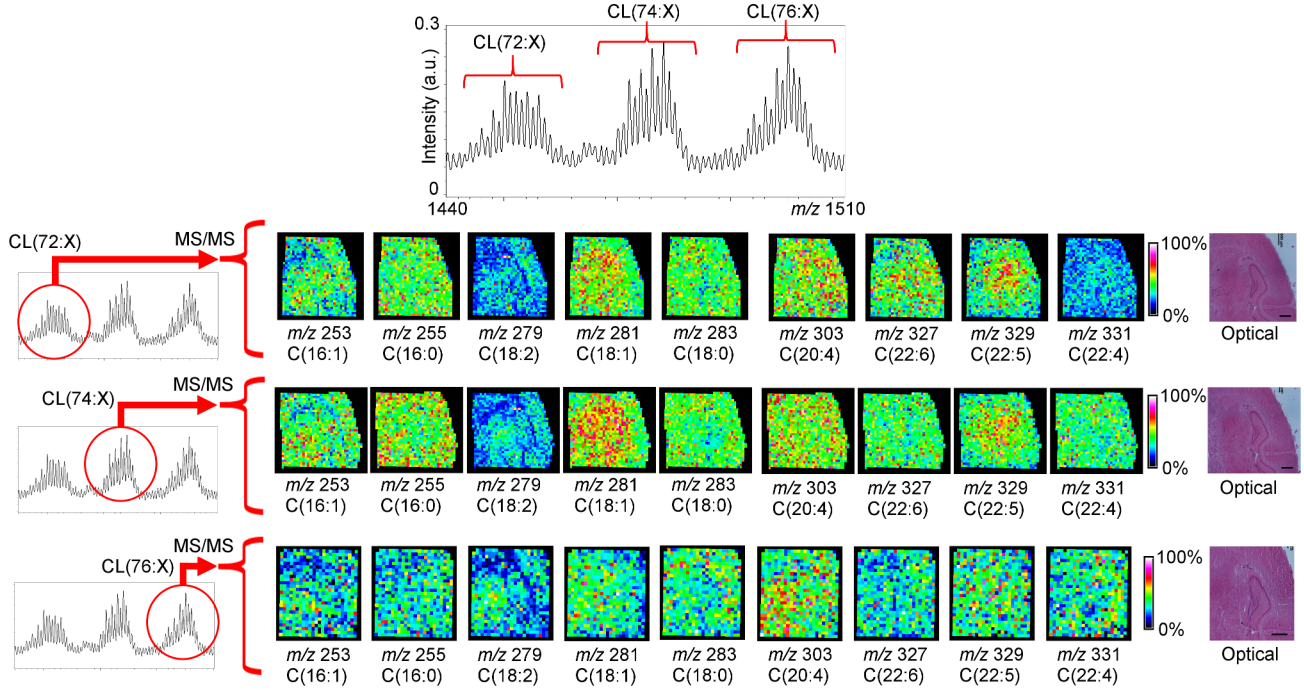

Figure 4. UltraFlextreme MALDI IMS analysis of fatty acyl fragments from the CL m/z 1448, 1476, and 1498 clusters. MS/MS analysis was performed on the CL clusters centered around m/z 1448 (72:X), 1476 (74:X), and 1498 (76:X). An optical image and heat maps (bar = 1 mm) for fragments of m/z 253, 255, 279, 281, 283, 303, 327, 329, and 331 are shown. Spatial resolution = 200 μm.

This region-specific expression of different CL species was also detectable at the single pixel (200 μm) level (Figure 2b) in diverse anatomical regions, including the medial dorsal thalamic nuclear (region A), the habenular nuclear (Hb) and dorsal third

dx.doi.org/10.1021/ac5011876 | Anal. Chem. 2014, 86, 6587−6595

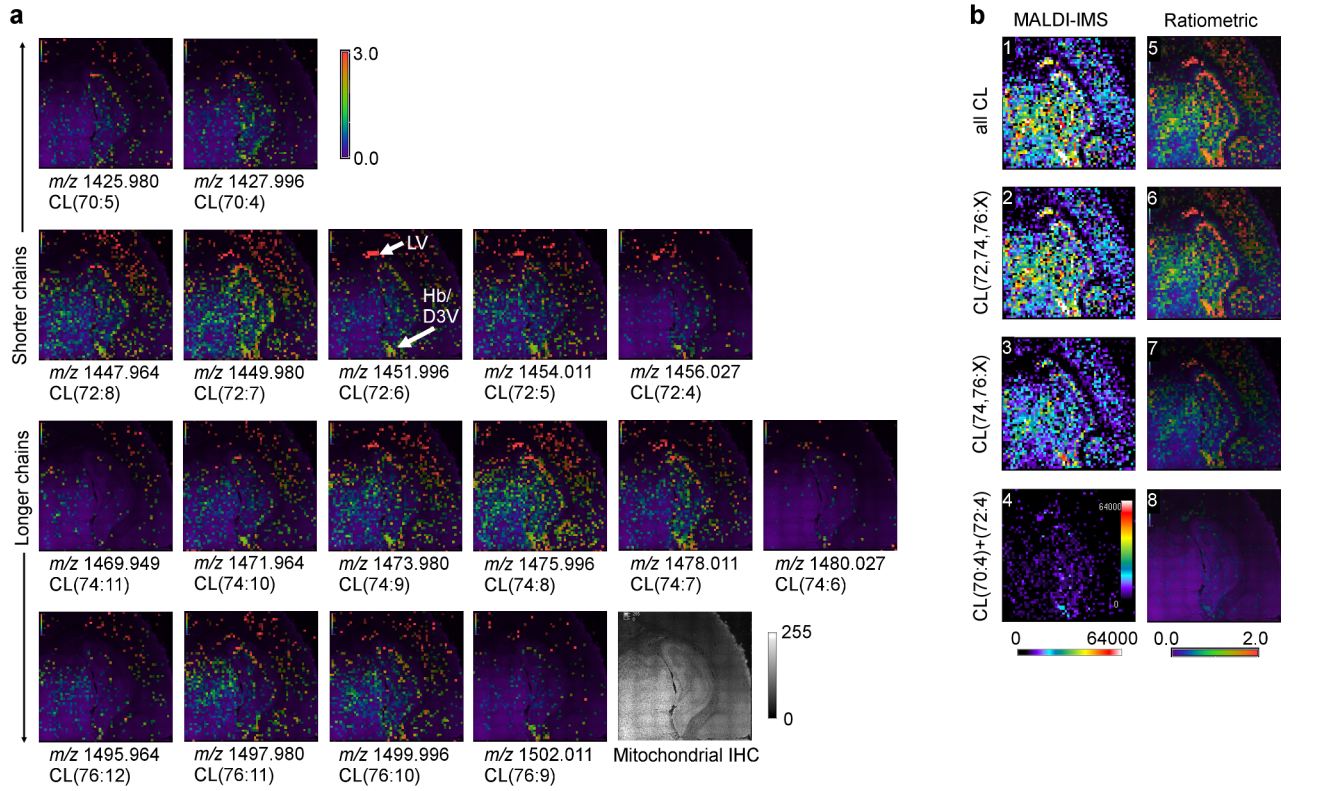

Figure 5. Ratiometric analysis of CL-IMS intensity to mitochondrial immunofluorescence intensity. Rat brain coronal sections (right hemispheres) were prepared for CL-IMS, and CL heat maps were generated. Semiserial brain sections were also prepared for mitochondrial immunohistochemical (IHC) staining using a fluorescent-labeled TOM 20 antibody. Ratiometric images for individual or grouped CL species are presented. (a) MS image intensities for 17 individual CL species were normalized to an 8 bit range and ratioed with the mitochondrial IHC image. Ratiometric images are displayed as a heat map on a scale from 0 (purple, less CL relative to mitochondria) to 3 (red, more CL relative to mitochondria). (b) CL-IMS groupings (panels 1−4) include: all CL species (All CL); CLs containing at least one PUFA of 18, 20, or 22 carbons (CL (72,74,76:X)); CLs containing at least one PUFA of 20 or 22 carbons (CL (74,76:X)); non-PUFA containing CLs of m/z 1427.996 [$(16:1)_1/(18:1)_3$] and 1456.027 [$(18:1)_4$]. These groupings are not normalized to the number of CL species; therefore, the absolute intensity will be highest in the heat map which includes all CL species. Ratioed images of CL groupings (panels 5−8) were rendered to a 12 bit range and displayed as heat maps on a scale from 0 (purple, less CL relative to mitochondria) to 2 (red, more CL relative to mitochondria).

ventricle (D3 V) (region B), the retrosplenial cortex (region C), the dentate gyrus (DG, region D), the external capsule white matter (region E), and the CA2 regions (region F). Notably, the medial dorsal thalamic nuclear region yielded a spectrum almost devoid of CL signal whereas the Hb/D3 V region was a CL "hot spot" with a robust signal centered around m/z 1474. We are certain that pixels without CL signals were not due to absence of matrix as signals for other lipids such as ST (m/z 806.5) and PI (m/z 885.5) were robust (Supplementary Figure 4, region A, Supporting Information). Spectra from the cortical, DG, and CA2 areas (region C, D, and F, Figure 2b) exhibited four major CL clusters centered around m/z 1450, 1474, 1500, and 1524. Regions A−F also exhibited robust phospholipid signals with differences in intensities relating to spatial locations (Supplementary Figure 4, Supporting Information).

Continued refinement of the mapping of CLs by FTICR MS (Solarix XR, FTICR, Bruker Daltonics, Billerica, MA) permitted us to (i) obtain images of 17 CL species at 100 μm resolution and to map a larger area encompassing the hippocampus and (ii) map masses for individual CL species to a 0.001 Da mass accuracy (Figure 3a). With this increased spatial resolution, four very low abundance CL species became undetectable. The CL species of m/z 1425.980 and 1427.996 were robust in the hippocampal location with a decreased density in the thalamus and cortex. CL species of m/z 1447.964 and 1449.980 had a similar distribution in the cortex, hippocampal, and thalamic areas with lower intensities for CLs of m/z 1451.996, 1454.011, and 1456.027. In addition, CL species of m/z 1447.964 displayed an intense signal in the Hb/D3 V area. Higher resolution imaging confirmed that the Hb/D3 V region was a consistent "hot spot" for CL and identified the lateral ventricle (LV) as an additional "hot spot" (see arrows). Overall, the thalamic, hippocampal, and cortical areas of the brain were enriched with asymmetrical (containing chiral carbons) polyunsaturated species such as CLs of m/z 1475.996, 1497.980, and 1499.996 in addition to the symmetrical tetralinoleoyl-CL (m/z 1447.964). CL spectra/images generated by FTICR were baseline resolved (Figure 3b,c; see also higher resolution images for other lipid species in Supplementary Figure 5, Supporting Information, and a complete listing of all accurate masses in Supplementary Table 2, Supporting Information).

MS/MS Analysis Maps CLs with Identified Fatty Acid Residues to Rat Brain Regions. To provide identification of CL species, we employed MS/MS analysis of CL clusters using a Bruker UltraFlextreme mass spectrometer (Bruker Daltonics, Billerica, MA) at 200 μm spatial resolution (Figure 4). An increased parent isolation window was needed to generate signals of sufficient intensity for fragmentation. Numerous fatty

dx.doi.org/10.1021/ac5011876 | Anal. Chem. 2014, 86, 6587−6595

acid fragments were detected including species with m/z 253 (C16:1), 255 (C16:0), 279 (C18:2), 281 (C18:1), 283 (C18:0), 303 (C20:4), 327 (C22:6), 329 (C22:5), and 331 (C22:4) within each CL cluster. The corresponding heat maps (Figure 4) are presented on a relative intensity scale to aid in displaying the spatial localization of very low abundance MS/MS fragments. In addition, typical phosphatidic acid (PA) fragments (a and b ions, m/z 695, 697, and 699) and lyso-PA fragments (m/z 415, 417, and 419), normally seen upon CL fragmentation, were evident (Supplementary Figures 6 and 7, Supporting Information).[30] The fragmentation analyses were in agreement with the IMS acquisitions for the CL parent ions. The linoleic acid fragment (m/z 279) from the 1476 cluster was more abundant in the thalamic and cortical regions than in the hippocampal formation (Figure 4). These results carried through with the fragmentation of the m/z 1448 and 1498 clusters. The intensity of the m/z 279 fragment from the various CL clusters was highest in the Hb/D3 V and LV areas confirming these regions as CL "hot spots". In addition, the C22:5 (m/z 329) fragment from different CL clusters was present at a higher level in the hippocampus, while the arachidonic acid (C20:4, m/z 303) fragment was more homogeneously distributed for all three CL clusters analyzed. Images for intermediate CL fragments are presented in Supplementary Figure 6, Supporting Information. The MS/MS fragmentation pattern for the CL cluster m/z 1474 was also confirmed on a lower resolution instrument (Bruker Ultraflex II) with results shown in Supplementary Figures 7 and 8, Supporting Information.

Ratiometric Analysis of CL/Mitochondria Displays Different Distributions of PUFA vs Non-PUFA Containing CLs. With the logical assumption that the relative distribution of individual CLs in mitochondria may vary among anatomical areas of the brain, we performed ratiometric analysis of CL images relative to mitochondrial abundance using immunohistochemical (IHC) imaging of mitochondria from semiserial sections (Figure 5a). Ratiometric data from the individual CL species are presented in Supplementary Table 3, Supporting Information. CL images were aggregated into 4 groupings: all CL, two PUFA groupings, and one non-PUFA grouping; ratiometric images were generated (Figure 5b). In general, IHC staining of mitochondria correlated very well with our IMS data. Overall, a higher CL/mitochondria ratio was found in the hippocampal area compared to the thalamus and cortex for most of the individual CL species (Figure 5a and Supplementary Table 3, Supporting Information). This was also evident in the resulting intensities displayed in the ratiometric image of all CL species (all CL, Figure 5b). Within the hippocampal area, the pyramidal cell layer, DG and CA3 regions displayed a high density of CL while the white matter region above the hippocampus displayed the lowest density of CL relative to mitochondria (Figure 5a,b).

In the brain, the extraordinary geographic diversification of CL may be associated with its two major functions: (i) structural organization of electron transport chain complexes and other mitochondrial membrane proteins and (ii) signaling.[3,5,8,31−33] It is believed that non-PUFA containing CL species (with saturated and monounsaturated acyls) and symmetric linoleoyl containing CL species mainly fulfill structural requirements, whereas longer chain PUFA containing CL species are used predominantly for signaling purposes.[3,5,8,31−33] Ratiometric analysis revealed that the non-PUFA containing CL species, m/z 1427.996 and 1456.027, mapped to a more central hippocampal location with CL/mitochondria ratios of 0.46 and 0.23, respectively (Figure 5a,b and Supplementary Table 3, Supporting Information). These non-PUFA containing CL species displayed extremely low intensities in the thalamic nuclear and cortical regions (Figure 5a,b and Supplementary Table 3, Supporting Information) but were present in the LV and Hb/D3 V areas. When the CLs consisting of at least one PUFA chain containing 18, 20, or 22 carbons (CL 72:X, 74:X, and 76:X) were grouped and ratiometric analysis was performed, much higher intensities were noted in the thalamus and cortical regions (Figure 5b). Similar ratiometric intensities for maps generated across the thalamic, hippocampal, and cortical regions were evident for CLs containing at least 20 or 22 carbon PUFA chains (Figure 5b). PUFA containing CL species also displayed a high CL/mitochondria ratio in the Hb/D3 V and LV areas (Figure 5a,b and Supplementary Table 3, Supporting Information). A general trend was noted within each CL cluster; essentially more saturated species also displayed a higher CL/mitochondrial ratio in the hippocampus relative to thalamus and cortex as compared to the more unsaturated CL species (Supplementary Table 3, Supporting Information). Overall, specific abundance patterns of PUFA containing vs non-PUFA containing CL species were revealed for different anatomical regions of the brain.

IMS offers a unique opportunity for label-free analysis of many types of individual phospholipids in tissue sections. The remarkable analytical power of this methodology has been successful for some lipid subclasses and in certain tissues where mitochondria (and hence CL) are truly abundant. For example, in cardiac tissue in which only a few CL isoforms predominate, detection has been recently achieved.[12,13] On the other hand in the brain, in which CLs are present at low abundance and with multiple isoforms, imaging has not been possible. Essentially, this tissue remained an IMS "terra incognita." Here, we show, for the first time, a MALDI-IMS technique that allows the imaging of important but low abundance CL species in different anatomical regions of the brain. Our employment of modified tissue protocols in conjunction with high mass accuracy FTICR instrumentation and MS/MS fragmentation analysis allows enhanced spatial resolution and identification of CL species in this difficult tissue. Recently, an imaging mass spectrometry study by Stutts et al. also utilized FTICR technology for the mapping of oxidized phosphatidylcholine species in spinal cord tissue.[34] While we did not detect any oxidized cardiolipin species from naïve brain tissue sections, our method is directly applicable to brain tissue sections from animals whose brain function has been compromised, such as from traumatic brain injury, an insult which has been shown to result in the production of CL oxidation products.[9]

CLs regulate various enzymatic activities in mitochondria and are essential components of dynamic supramolecular complexes (respirasomes).[31−33,35] Moreover, individual mitochondria may display different bioenergetic-specific requirements for specific CLs as described for murine brain tissue.[36] In the brain, energy usage is dictated by (a) region-specific metabolic demands, (b) the response to a particular stimulus (signaling), and (c) the developmental stage of the tissue.[33] Accordingly, when all of the CL species detected by IMS were integrated and ratiometric analysis was performed, a clear correlation was found between CL and a mitochondrial integral membrane protein TOM 20. These data are in agreement with previous studies of other mitochondrial markers like cytochrome oxidase (CO) in rat

dx.doi.org/10.1021/ac5011876 | Anal. Chem. 2014, 86, 6587−6595

brain,[37] whereby a low CO activity in the medial dorsal thalamic nuclear region (our region A, Figure 2), a moderate CO activity in the hippocampal formation (our region D, Figure 2), and an unusually high degree of reactivity in the Hb nuclear area (our CL "hot spot", region B, Figure 2) were detected.

The amazing spatial diversification of different CL isoforms in the brain is numerically far greater than that seen in other tissues.[38] Moreover, the abundance of the long-chain PUFA species in the brain cannot be explained exclusively by the bioenergetic demands. Indeed, the diversity of CL isoforms in the mitochondria of many highly effective ATP-generating tissues is very limited, mostly limited to saturated and mono- and diunsaturated fatty acid residues. It has been suggested, but never experimentally proven, that tetra-, penta-, and hexaenoic CL species fulfill other fundamental, signaling functions in the brain.[8,38] Our IMS data demonstrate, for the first time, the heterogeneity of PUFA containing and non-PUFA containing CLs in different anatomical areas of the brain. Combined with our previously demonstrated role for PUFA-CLs as precursors of lipid mediators,[8] our data provides direct experimental evidence for the concept of CL-dependent signaling via the generation of lipid mediators. The CL species, which we have mapped to the thalamic and hippocampal areas which contain arachidonoyl and docosahexanoyl fatty acid chains (m/z 1473.977, 1475.991, 1478.010, 1495.963, 1497.979, and 1499.995), would inevitably serve as excellent substrates for these types of signaling lipids. We have also defined the LV as an additional CL "hot spot", whereby the PUFA containing CL species (m/z 1473.976 and 1475.991) may also serve as a source of signaling lipid mediators. The latter region-specific CL species from the choroid plexus (CP)/LV area contains one or more 20:4 acyls which may serve as precursors to thromboxanes (TXs), the major signaling lipid produced by the CP.[39] Many of the PUFA containing CL species we have detected display a higher CL/mitochondrial ratio within the hippocampal formation. Given the role of the hippocampus in learning, memory, and spatial navigation, it is tempting to speculate that these diversified PUFA-CLs are needed to fulfill signaling roles essential for homeostatic and regulatory functions involving cellular proliferation, differentiation, and synaptogenesis.[8,39−42]

The ability to perform MS/MS analysis underlies the detailed verification of region-specific fatty acyl compositions of CLs in brain tissue as it relates to CLs as a source of lipid mediators. We have shown that, when fragmented, many of the CL clusters which contain C20:4, C22:5, and C22:6 acyls (m/z 303, 329, and 327, respectively) display a widespread though specific distribution in the thalamic, hippocampal, and cortical regions. These PUFA containing CL species are potentially susceptible to attack by *cyt c*/H_2O_2 and release by PLA_2 hydrolysis that can lead to a variety of lipid mediators in these areas of the brain.[8]

CONCLUSIONS

In conclusion, we have been able to map individual CL molecular species in brain tissue sections using our modified tissue protocol and demonstrate, for the first time, the heterogeneity of PUFA containing and non-PUFA containing CLs in different anatomical regions of the brain. In addition, we have defined the LV and Hb/D3 V areas of the brain as CL "hot spots". Finally, our modified protocol also allowed us to map the fatty acyl profiles of several CL clusters to various brain regions. Our novel method for the imaging of various CL species and their fatty acyl compositions in the brain offers new opportunities to obtain insights into a number of biologically intriguing questions concerning the involvement of CL in signaling, development, and function in normal and injured tissue.

ASSOCIATED CONTENT

Supporting Information

Additional materials as described in the text. This material is available free of charge via the Internet at http://pubs.acs.org

AUTHOR INFORMATION

Corresponding Authors

*E-mail: amoscatoaa@upmc.edu.
*E-mail: bayihx@ccm.upmc.edu.
*E-mail: kagan@pitt.edu.

Author Contributions

#A.A.A. and L.J.S. contributed equally to the work.

Notes

The authors declare no competing financial interest.

ACKNOWLEDGMENTS

This work was supported by NIH: ES020693, ES021068, U19AI068021, NS076511, and NS061817; NIOSH OH008282; P01 HL114453; U54 GM103529 08 (S.W.) and had partial support from Fulbright Canada (V.E.K.). This project used the UPCI Cancer Biomarkers Facility supported in part by Cancer Center Support Grant (CCSG) P30CA047904. The authors would like to thank J. Lewis for his technical assistance in tissue sectioning.

REFERENCES

(1) Hoch, F. L. *Biochim. Biophys. Acta* **1992**, *1113*, 71−33.
(2) Kagan, V. E.; Bayir, H. A.; Belikova, N. A.; Kapralov, O.; Tyurina, Y. Y.; Tyurin, V. A.; Jiang, J.; Stoyanovsky, D. A.; Wipf, P.; Kochanek, P. M.; Greenberger, J. S.; Pitt, B.; Shvedova, A. A.; Borisenko, G. *Free Radical Biol. Med.* **2009**, *46*, 1439−1453.
(3) Claypool, S. M.; Koehler, C. M. *Trends Biomed. Sci.* **2011**, *37*, 32−41.
(4) Schlame, M. *J. Lipid Res.* **2008**, *49*, 1607−1620.
(5) Osman, C.; Velker, D. R.; Langer, T. *J. Cell Biol.* **2011**, *192*, 7−16.
(6) Schlattner, U.; Tokarska-Schlattner, M.; Ramirez, S.; Tyurina, Y. Y.; Amoscato, A. A.; Mohammadsanyi, D.; Huang, Z.; Jiang, J.; Yanamala, N.; Seffouh, A.; Boissan, M.; Epand, R. F.; Epand, R. M.; Klein-Seetharaman, J.; Lacombe, M.-L.; Kagan, V. E. *J. Biol. Chem.* **2013**, *288*, 111−121.
(7) Chu, C. T.; Ji, J.; Dagda, R. K.; Jiang, J. F.; Tyurina, Y. Y.; Kapralov, A. A.; Tyurin, V. A.; Yanamala, N.; Shrivastava, I. H.; Mohammadyani, D.; Wang, K. Z. Q.; Zhu, J.; Klein-Seetharaman, J.; Balasubramanian, K.; Amoscato, A. A.; Borisenko, G.; Huang, Z.; Gusdon, A. M.; Cheikhi, A.; Steer, E. K.; Wang, R.; Baty, C.; Watkins, S.; Bahar, I.; Bayır, H.; Kagan, V. E. *Nat. Cell Biol.* **2013**, *15*, 1197−1205.
(8) Tyurina, Y. Y.; Poloyac, S. M.; Vikulina, A. S.; Jung, M.-Y.; Tyurin, V. A.; Kapralov, A. A.; Epperly, M. W.; Greenberger, J. S.; Vladimirov, Y. A.; Bayir, H.; Kagan, V. E. *Nat. Chem.* **2014**, *6*, 542−552.
(9) Bayir, H.; Tyurin, V. A.; Tyurina, Y. Y.; Viener, R.; Ritov, V.; Amoscato, A. A.; Zhao, Q.; Zhang, X.; Feldman-Janesko, K. L.; Alexander, H.; Clark, R. S. B.; Kochanek, P. M.; Kagan, V. E. *Ann. Neurol.* **2007**, *62*, 154−169.
(10) Tyurin, V. A.; Tyurina, Y.; Feng, W.; Mnuskin, A.; Jiang, J.; Tang, M.; Zhang, X.; Zhao, Q.; Kochanek, P. M.; Clark, R. S.; Bayir, H.; Kagan, V. E. *J. Neurochem.* **2008**, *107*, 1614−1633.

(11) Wang, H.-Y. J.; Jackson, S. N.; Woods, A. S. *J. Am. Soc. Mass Spectrom.* **2007**, *18*, 567−577.
(12) Jackson, S. N.; Baldwin, K.; Muller, L.; Womack, V. M.; Schultz, J. A.; Balaban, C.; Woods, A. S. *Anal. Bioanal. Chem.* **2013**, DOI: 10.1007/s00216-013-7525-6.
(13) Wang, H. Y.; Wu, H. W.; Tsai, P. J.; Liu, C. B.; Zheng, Z. F. *Anal. Bioanal. Chem.* **2014**, *406*, 565−575.
(14) Ji, J.; Kline, A. E.; Amoscato, A.; Arias, A. S.; Sparvero, L. J.; Tyurin, V. A.; Tyurina, Y. Y.; Fink, B.; Cheng, J. P.; Alexander, H.; Clark, R. S. B.; Kochanek, P. M.; Wipf, P.; Kagan, V. E.; Bayır, H. *Nat. Neurosci.* **2012**, *15*, 1407−1415.
(15) Kagan, V. E.; Tyurin, V. A.; Jiang, J.; Tyurina, Y. Y.; Ritov, V. B.; Amoscato, A. A.; Osipov, A. N.; Belikova, N. A.; Kapralov, A. A.; Kini, V.; Vlasova, I. I.; Zhao, Q. M.; Zou, M.; Di, P.; Svistunenko, D. A.; Kurnikov, I. V.; Borisenko, G. G. *Nat. Chem. Biol.* **2005**, *1*, 223−232.
(16) Paxinos, G.; Watson, C. *The Rat Brain in Sterotaxic Coordinates*; Academic Press, Inc.: San Diego, California, USA, 1997.
(17) Samhan-Arias, A. K.; Ji, J.; Demidova, O. M.; Sparvero, L. J.; Feng, W.; Tyurin, V.; Tyurina, Y. Y.; Epperly, M. W.; Shvedova, A. A.; Greenberger, J. S.; Bayır, H.; Kagan, V. E.; Amoscato, A. A. *Biochim. Biophys. Acta* **2012**, *1818*, 2413−2423.
(18) Watkins, S. Immunohistochemistry. In *Current Protocols in Cytometry*; John Wiley & Sons, Inc.: Hoboken, NJ, 2009; Chapter 12, Unit 12.16; DOI: 10.1002/0471142956.cy1216s48.
(19) Sparvero, L. J.; Amoscato, A. A.; Kochanek, P. M.; Pitt, B. R.; Kagan, V. E.; Bayir, H. *J. Neurochem.* **2010**, *115*, 1322−1336.
(20) Norris, J. L.; Caprioli, R. M. *Chem. Rev.* **2013**, *113*, 2309−2342.
(21) Chen, Y.; Allegood, J.; Liu, Y.; Wang, E.; Cachon-Gonzalez, B.; Cox, T. M.; Merrill, A. H., Jr.; Cameron Sullards, M. *Anal. Chem.* **2008**, *80*, 2780−2788.
(22) Fuchs, B.; Süß, R.; Schiller, J. *Prog. Lipid Res.* **2010**, *49*, 450−475.
(23) Goto-Inoue, N.; Hayasaka, T.; Zaima, N.; Setou, M. *Biochim. Biophys. Acta, Mol. Cell Biol. Lipids* **2011**, *1811*, 961−969.
(24) Hankin, J.; Farias, S.; Barkley, R.; Heidenreich, K.; Frey, L.; Hamazaki, K.; Kim, H.-Y.; Murphy, R. *J. Am. Soc. Mass Spectrom.* **2011**, *22*, 1014−1021.
(25) Landgraf, R. R.; Garrett, T. J.; Prieto Conaway, M. C.; Calcutt, N. A.; Stacpoole, P. W.; Yost, R. A. *Rapid Commun. Mass Spectrom.* **2011**, *25*, 3178−3184.
(26) Angel, P. M.; Spraggins, J. M.; Baldwin, H. S.; Caprioli, R. *Anal. Chem.* **2012**, *84*, 1557−1564.
(27) Johanson, R. A.; Buccafusca, R.; Quong, J. N.; Shaw, M. A.; Berry, G. T. *Anal. Biochem.* **2007**, *362*, 155−167.
(28) Colsch, B.; Jackson, S. N.; Dutta, S.; Woods, A. S. *ACS Chem. Neurosci.* **2011**, *2*, 213−222.
(29) Colsch, B.; Woods, A. S. *Glycobiology* **2010**, *20*, 661−667.
(30) Hsu, F.-F.; Turk, J.; Rhoades, E. R.; Russell, D. G.; Shi, Y.; Groisman, E. A. *J. Am. Soc. Mass Spectrom.* **2005**, *16*, 491−504.
(31) Bazan, S.; Mileykovskaya, E.; Mallampalli, V. K. P. S.; Heacock, P.; Sparagna, G. C.; Dowhan, W. *J. Biol. Chem.* **2013**, *288*, 401−411.
(32) Winge, D. R. *Mol. Cell. Biol.* **2012**, *32*, 2647−52.
(33) Wirtz, S.; Schuelke, M. *PLoS One* **2011**, *6*, 1−12.
(34) Stutts, W. L.; Menger, R. F.; Kiss, A.; Heeren, R. M. A.; Yost, R. A. *Anal. Chem.* **2013**, *85*, 11410−11419.
(35) Rosca, M.; Minkler, P.; Hoppel, C. L. *Biochim. Biophys. Acta* **2011**, *1807*, 1373−82.
(36) Ta, N. L.; Jia, X.; Kiebish, M.; Seyfried, T. N. *Lipids* **2014**, *49*, 113−117.
(37) Hevner, R. F.; Lui, S.; Wong-Riley, M. T. T. *Neuroscience* **1995**, *65*, 313−342.
(38) Kiebish, M. A.; Bell, R.; Kui Yang, K.; Phan, T.; Zhao, Z.; Ames, W.; Seyfried, T. N.; Gross, R. W.; Chuang, J. H.; Han, X. *J. Lipid. Res.* **2010**, *51*, 2153−2170.
(39) Farooqui, A. In *Lipid Mediators and Their Metabolism in the Brain*; Springer Science and Business Media: New York, 2011; pp 1−48.
(40) Schlame, M.; Horwath, L.; Vigh, L. *Biochem. J.* **1994**, *265*, 79−85.
(41) Kann, O.; Kovacs, R. *Am. J. Physiol. Cell Physiol.* **2007**, *292*, C641−C657.
(42) Jarrard, L. E. *Behav. Neural Biol.* **1993**, *60*, 9−26.